Collective bubble dynamics near a surface in a weak acoustic standing wave field

Xiaoyu Xi and Frederic Cegla[a)]
Department of Mechanical Engineering, Imperial College London, London SW7 2AZ, United Kingdom

Robert Mettin
Christian Doppler Laboratory for Cavitation and Micro-Erosion, Drittes Physikalisches Institut, Georg-August-Universität Göttingen, Friedrich-Hund-Platz 1, 37077 Göttingen, Germany

Frank Holsteyns and Alexander Lippert
Lam Research AG, SEZ-Strasse 1, 9050 Villach, Austria

(Received 7 February 2012; revised 2 May 2012; accepted 3 May 2012)

The transport of bubbles to a neighboring surface is very important in surface chemistry, bioengineering, and ultrasonic cleaning, etc. This paper proposes a multi-bubble transport method by using an acoustic standing wave field and establishes a model that explains the multi-bubble translation by expressing the balance between Bjerknes forces and hydrodynamic forces on a bubble in a liquid medium. Results indicated that the influence of primary Bjerknes force, secondary Bjerknes force, and buoyancy force on the bubble translation depends on the position of the target bubble in the acoustic field. Moreover, it was found that increasing the size of a bubble or pressure amplitude can accelerate the bubble motion and enhance the bubble-bubble interaction. The secondary Bjerknes force between two bubbles can switch from an attractive one when they oscillate in phase to a repulsive one when the bubble oscillations are out of phase. These findings provide an insight into the multi-bubble translation near a surface and can be applied to future bubble motion control studies, especially in drug delivery, sonoporation, and ultrasonic cleaning.
 [http://dx.doi.org/10.1121/1.4726009]

PACS number(s): 43.25.Yw, 43.20.Ks, 43.35.Yb, 43.25.Qp [TDM] Pages: 37–47

I. INTRODUCTION

It has been recognized that acoustically driven bubbles can trigger substantial physical and chemical effects on a neighboring surface.[1,2] Extensive experimental investigations have been carried out during the past few decades to understand the interactions between cavitation bubbles and surfaces of different properties, from a solid plane surface[3] to an elastic membrane.[4,5] It was found that the liquid jet that is formed during the collapse of a bubble near a boundary is responsible for a range of bubble induced physical and chemical reactions, and such liquid motion is strong enough to erode a solid surface[6] or clean contaminated wafers.[7–9] Numerical calculations of cavitation bubbles near a boundary are also found in the literature.[10–12] Lauterborn and Kurz recently published a comprehensive review of this topic.[13]

Despite the successful investigations of interactions between cavitation bubbles and a surface, only recently has the study of the acoustic response of moderately oscillating bubbles near a surface started to attract more and more attention due to its importance in understanding sonoporation and drug delivery. At a low pressure amplitude, a bubble experiences a moderate oscillation and consequently induces a flow circulation around it. The oscillation is assumed to be capable of gently disturbing the fluid flow near a surface or opening breaches on cell membranes.[14] Marmottant *et al.*[15–17] explored the micro flow circulation generated by a bubble attaching to a solid surface. The change in micro-bubble dynamics near a solid wall was revealed by Garbin *et al.*[18] Meanwhile, Vos *et al.*[19,20] experimentally investigated the deformed radial oscillation of a micro-bubble on a cellulose wall. Besides these experimental studies, a series of numerical analyses was carried out by Doinikov[21–23] to explain the acoustic response of ultrasound contrast agents (UCAs) near a boundary, especially the shear stress generated by an UCA on a surface that is believed to be the mechanism of bubble induced sonoporation or cell lysis. However, direct correlation between bubble oscillation and the consequent biological reactions has not yet been quantified. Moreover, in the mentioned studies, cavitation bubbles were normally generated near a target surface by a focused laser beam. Such approach, however, is difficult to accurately control the force generated by the target bubbles. As an alternative solution, oscillating bubbles are required to be transported to a surface within a short time. Therefore there is a need to explore the means to effectively transport a large amount of bubbles to an appointed location on a designed trajectory and to manipulate the bubble oscillation in a controlled manner.

The motion of a bubble in a bulk liquid medium is controlled by acoustic and hydrodynamic forces simultaneously. A gas bubble driven below its resonance frequency in a weak standing wave field moves toward the pressure anti-node,

a)Author to whom correspondence should be addressed. Electronic mail: f.cegla@imperial.ac.uk

while a bubble driven above its resonance frequency moves toward the pressure node instead. This effect is attributed to the primary Bjerknes force on a bubble and has been studied extensively by several authors.[24–28] The bubble habitant in an acoustic standing wave field was recently studied by Koch *et al.*[29] Besides the primary Bjerknes force generated by an imposed acoustic field, the translation of a bubble can also be influenced by boundary conditions or neighboring oscillating bubbles, which exert secondary Bjerknes forces on the target bubble. The secondary Bjerknes force takes effect between two nearby bubbles because the force is inversely proportional to the square of the separation distance between two bubbles.[30,31] A bubble can exert either an attractive or a repulsive secondary Bjerknes force on a neighboring one, depending on the driving frequency and the bubble sizes.[32] By taking the bubble-bubble interaction into account, the formation of a bubble cluster in an acoustic standing wave resonator was successfully simulated by Mettin *et al.*[33] and Parlitz *et al.*[34] Doinikov,[35] however, later pointed out that a missing term in Mettin's and Parlitz's works may make their model inadequate in other applications and therefore proposed a more comprehensive model by using a Lagrangian formalism. Apart from these studies, however, little is known of the influence of secondary Bjerknes forces on the translation of a bubble near a surface in a multi-bubble environment. It was the aim of the present study to develop an experimental configuration to investigate the effects of different acoustic and hydrodynamic forces on the bubble translation near a boundary.

Recently, the authors reported a multi-layered resonator for controlling single bubble translation near a surface in an acoustic standing wave field.[36] The resonator can create an uniform one-dimensional standing wave field in a liquid medium. The acoustic characteristics of such a structure (impedance and pressure distribution) were successfully predicted by a one-dimensional equivalent network model (1D model).[37,38] In this paper, the translation of bubbles in a more general multi-bubble environment is presented, and the dynamics of bubbles in a weak acoustic standing wave field are discussed in more detail.

This paper is organized as follows. In Sec. II, details of the experimental setup are described. Section III provides the theoretical background of the bubble translation in a multi-bubble environment. In Sec. IV, experimental results obtained from a high speed camera are shown and are explained by the bubble translation model in Sec. V. Conclusions are drawn in Sec. VI.

II. EXPERIMENTAL CONFIGURATION

It is well known that a bubble can move in an acoustic standing wave field either toward a pressure node or a pressure anti-node, depending on the bubble size and the driving frequency. In this study, the standing wave was created by a multi-layered resonator and the motion of bubbles, which were generated by an electrolysis method, was recorded by a high speed camera system.

The main parts of the resonator are a liquid (deionized water) cube held in a brass block (length * width * thickness = 10 mm × 10 mm × 8 mm) and a round transducer with diameter of 10 mm (Fig. 1). The origin of the coordinate system ($x = 0$ mm, $y = 0$ mm, $z = 0$ mm) was set at the center of the transducer-liquid interface. To make it possible to optically observe the inside of the cell, the cross section of the water layer was chosen as a square shape (10 mm × 10 mm), and two glass windows were fitted on both sides of the liquid medium. Because the aim of the present work is to investigate the bubble behavior near a surface, a round borosilicate glass plate (glass 1) of 0.1 mm thickness (VWR, UK) was placed at $x = 4$ mm as the target surface, and another glass plate (glass 2 at $x = 8$ mm) was used to confine the liquid within the structure.

The transducer was fabricated out of a lead zirconate titanate (PZT) disk (PCM 51, EP Electronic Components Ltd., UK), a backing brass bar, a front brass bar with thickness of 4, 13, and 15 mm, respectively.

An electrolysis method was used to generate bubbles of radii ranging from 10 to 50 μm. Two wires (tin-coated copper) were connected to a DC power supply (TNG 35, Voltcraft, Germany), and the electrical potential was set to 5 V. The free ends of the wires were placed at $x = 5$ mm as shown in Fig. 1. It was found that when the sound field was switched off, bubbles could freely float away from the tip of the tin-coated copper wire and form a chain of bubbles. However, in the presence of an acoustic field, the bubbles accumulate at the wire tip. To prevent the coalescence of bubbles, the bubbles used in the experiments were generated before the sound field was on.

The bubble motion was recorded by a high speed camera (FastCam SA5, Photron, USA) at a frame rate of 100 000 frames/s. A viewing window with size of 3 mm × 1.8 mm was chosen to cover the cross section of glass 1 ($x = 4$ mm) and the bubble injection point ($x = 5$ mm) at the same time. The recorded bubble translation as a function of time was analyzed by an object tracking algorithm written in MATLAB (Mathworks Inc., USA). The dimensions of objects in a video were calibrated with a standard 300 μm width stick.

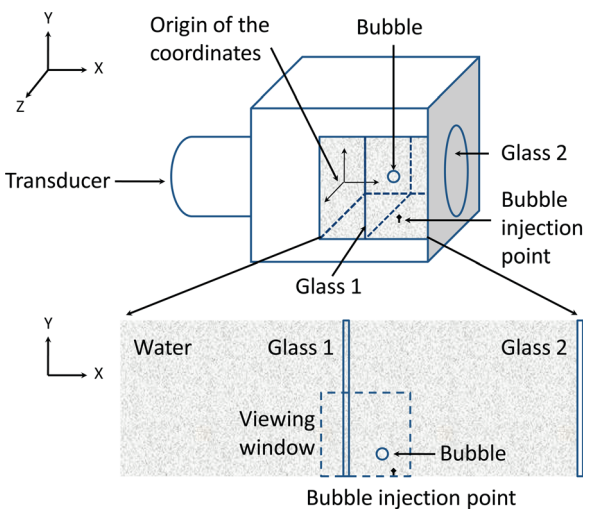

FIG. 1. (Color online) A schematic diagram of the multi-layered resonator for multi-bubble transport.

III. BUBBLE TRANSLATION MODEL

When a bubble moves within the resonator (Fig. 1), its motion is controlled by acoustic and hydrodynamic forces simultaneously. A schematic diagram of the multi-bubble environment is shown in Fig. 2, and Fig. 3 demonstrates the relationship between different external forces on a target bubble (bubble 1). The translation of bubble 1 is mainly influenced by the imposed acoustic field, the boundary surfaces (glasses 1 and 2), a nearby bubble 2, and the buoyancy force from the surrounding liquid.

In the multi-bubble environment, the bubble translation is influenced by the primary Bjerknes force (F_p) generated by the acoustic field in the x axis,[39]

$$F_p = -\frac{4\pi}{3} R_n^3 k P_a \sin(\omega t)\cos(kd_n) \tag{1}$$

where R_n is the radius of the nth bubble, P_a is the pressure amplitude, ω is the angular frequency, t is time, and k is the wave number. d_n is the distance between the center of the nth bubble and a pressure anti-node along the x axis in Fig. 2.

Glass 1 and 2 exert attractive secondary Bjerknes forces on bubble 1. Mathematically, the attractive forces can be represented by introducing imaginary bubbles on the opposite side of the surfaces. In Fig. 2, for example, bubble 1 and an imaginary bubble (bubble 3), which oscillates in phase with its counterpart, are placed equally on each side of glass 1. Moreover, the nearby bubble 2 can exert either an attractive secondary Bjerknes force on bubble 1 when they oscillate in phase or a repulsive force when their oscillations are out of phase at the driving frequency.

It needs to be pointed out here that in a strict mathematical sense, the oscillation of a bubble between two rigid walls is represented by an array of an infinite number of imaginary bubbles that are symmetrically located on the other sides of the walls. In the present study, only the first approximation is considered to represent the whole system. Such an approximation is justified by the fact that the influence of the imaginary bubbles on the target bubble strongly depends on the separation distance between the bubbles. Krasovitski *et al.*[40] simulated the extreme case where a bubble collapses very close to two rigid boundaries. The walls

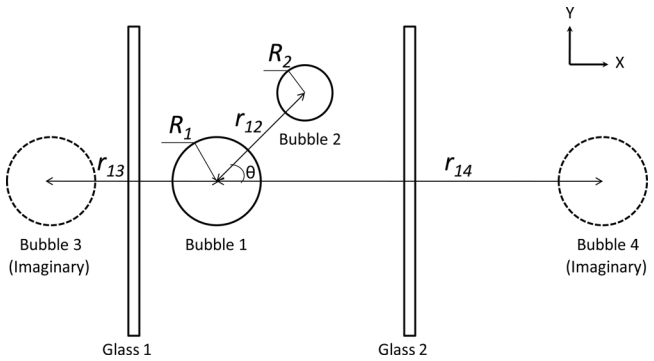

FIG. 2. The position relationship between a bubble and its imaginary counterparts and a neighboring bubble in a sound field.

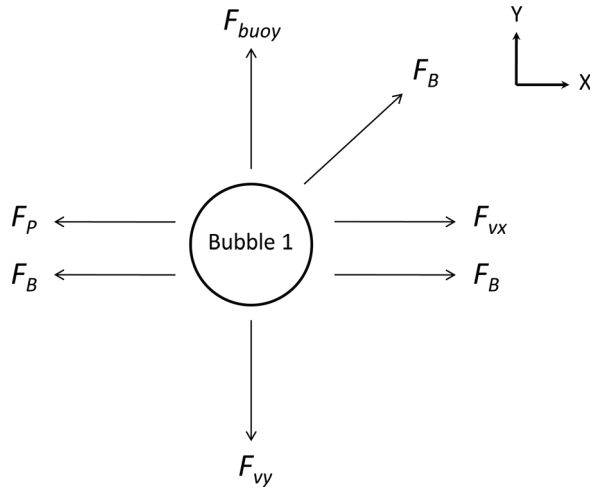

FIG. 3. The relationship between different external forces on bubble 1.

are located at a distance of the same order of the bubble diameter. Their results indicated that, however, only three pairs of imaginary bubbles are needed to provide a good accuracy of the bubble collapse, while the influence from the mirror bubbles located in the far field can be neglected. In our case, the bubble radii ranged from 10 to 50 μm. Initially, the bubbles were 1 mm away from one surface and 3 mm from the other. These separation distances were at least 10 times more than the bubble diameter. Thus only the first approximation of a single imaginary bubble is required to obtain an accurate solution.

For a pair of bubbles, if the bubble shapes are assumed to remain spherical for all time with the radii R_1 and R_2, respectively, the respective pressure, for example, generated from bubble 2 on bubble 1, is given by[32]

$$p = \frac{\rho}{r_{12}} \frac{\mathrm{d}}{\mathrm{d}t} R_2^2 \dot{R}_2 \tag{2}$$

where r_{12} is the separation distance between the two bubbles. ρ is the liquid density. The overdot denotes the time derivative.

The secondary Bjerknes force between the bubbles is given by[32]

$$F_B = -\frac{\rho}{4\pi r_{12}^2} \langle \dot{V}_1 \dot{V}_2 \rangle \tag{3}$$

where V_1 and V_2 are the volume of bubbles 1 and 2, respectively. $\langle\rangle$ denotes the time average.

Besides Bjerknes forces, the bubbles experience drag and buoyancy forces from the surrounding liquid. The drag forces in the x (F_{vx}) and y (F_{vy}) axes are given by[39]

$$F_{vx} = -12\pi\eta R_n(\dot{x}_n - v_e), \tag{4}$$

$$F_{vy} = -12\pi\eta R_n \dot{y}_n \tag{5}$$

where η is the liquid viscosity. x_n and y_n are the positions of the nth bubble center on the x and y axes. v_e is the liquid

velocity that is generated by the imposed acoustic field at the center of the bubble

$$v_e = \frac{P_a}{\rho c}\cos(\omega t)\cos(kd_n) \tag{6}$$

where c is the liquid velocity. Here a plane standing wave is assumed and boundary layers at walls are neglected.

The buoyancy force in the y axis is

$$F_{buoy} = \frac{4\pi}{3}R_n^3(\rho - \rho_{gas}) \tag{7}$$

where ρ_{gas} is the density of gas inside a bubble.

Therefore the translational equations of the nth bubble in a multi-bubble environment are given by[41]

$$\ddot{x}_n + \frac{3\dot{R}_n\dot{x}_n}{R_n} = \frac{3F_{ex}}{2\pi\rho R_n^3}, \tag{8}$$

$$\ddot{y}_n + \frac{3\dot{R}_n\dot{y}_n}{R_n} = \frac{3F_{ey}}{2\pi\rho R_n^3} \tag{9}$$

where F_{ex} and F_{ey} are the external forces in the x axis and y axis, respectively. F_{ex} represents the forces in the x axis that are equal to the sum of the primary Bjerknes force (F_p), the viscous drag force (F_{vx}) and the x axis component of the secondary Bjerknes forces ($F_B\cos\theta$ in Fig. 2), which includes the forces generated by the boundaries and neighboring bubbles. F_{ey} is the sum of buoyancy force (F_b), viscous force (F_{vy}), and the y axis component of the secondary Bjerknes forces $F_B\sin\theta$ (including the influences from the boundaries and neighboring bubbles in Fig. 2).

Furthermore, the time-varying bubble radius is calculated based on the Keller–Miksis equation.[42] In a multi-bubble environment, the Keller–Miksis equation needs to be expanded to include the influences from the boundary conditions and neighboring bubbles. By incorporating Eq. (2) into the Keller–Mikisis equation, the oscillation of the nth bubble is obtained:

$$\left(1-\frac{\dot{R}_n}{c}\right)R_n\ddot{R}_n + \left(\frac{3}{2}-\frac{\dot{R}_n}{2c}\right)\dot{R}_n^2 - \frac{1}{\rho}\left(1+\frac{\dot{R}_n}{c}\right)P_{sc} - \frac{R_n}{\rho c}\dot{P}_{sc} = \frac{\dot{x}_n^2}{4} - \sum_{\substack{m=1\\ m\neq n}}^{N}\frac{1}{r_{nm}}(2\dot{R}_m^2R_m + R_m^2\ddot{R}_m), \tag{10}$$

$$P_{sc} = \left(P_0 + \frac{2\sigma}{R_{n0}}\right)\left(\frac{R_{n0}}{R_n}\right)^{3\gamma} - \frac{2\sigma}{R_n} - \frac{4\eta\dot{R}_n}{R_n} - P_0 - P_{ex} \tag{11}$$

where R_{n0} is the equilibrium radius of the nth bubble, and an ensemble of N bubbles is considered. r_{nm} is the distance between the center of the nth and mth bubbles. P_0 is the hydrostatic pressure, σ is the surface tension, γ is the polytropic exponent of the gas within the bubble. The majority of the bubbles used in the experiments were driven far below their resonance frequencies. The bubble sizes were relatively small compared to the wavelength of the driving signal; this means the bubbles were supposed to behave isothermally. P_{ex} is the external driving signal that is defined as a standing wave here:

$$P_{ex} = P_a\sin(\omega t)\sin(kd_n). \tag{12}$$

The left terms of Eq. (10) are the modified Keller–Miksis equation for the nth bubble. This modified Keller–Miksis equation is coupled to the velocity of the nth bubble through the first term on the right and to the pressure emitted or scattered by the neighboring bubbles through the second term on the right.

The resonance frequency of a bubble is[39]

$$f_{res} = \frac{1}{2\pi R_0}\sqrt{\frac{3\gamma P_0}{\rho}\left(1+\frac{2\sigma}{P_0R_0}\right) - \frac{2\sigma}{R_0\rho}}. \tag{13}$$

A total velocity is defined here as a function of time:

$$v_{total}(t) = \sqrt{\dot{x}_n^2(t) + \dot{y}_n^2(t)}. \tag{14}$$

IV. RESULTS

In this section, the measured acoustic standing wave field and observed bubble translations within the resonator are shown. The values of the physical parameters used in this study are $f = 46.8$ kHz, $\rho = 1000$ kg/m^3, $P_0 = 101.3$ kPa, $c = 1480$ m/s, $\sigma = 0.072$ N/m, $\gamma = 1$, $\eta = 0.001$ Pa s. Experimental videos were recorded within a 3 mm× 1.8 mm viewing window at a frame rate of 100 000 frames/s.

A. The acoustic standing wave field

It has been shown in a previous work[36] that the one-dimensional equivalent electrical network of a transducer (1D model) is suitable for quantifying the pressure distribution of the present resonator. A simulated pressure distribution of the water layer with glass 1 at 46.8 kHz is displayed in Fig. 4 for input signal amplitude of 4 V (peak). It can be seen from Fig. 4 that a calculated maximum pressure amplitude of 11.5 kPa is located at the origin of the coordinate system ($x = 0$ mm in Fig. 1), and the pressure amplitude gradually drops to a minimum at the boundary between the water layer and glass 2 ($x = 8$ mm) as indicated in Fig. 4.

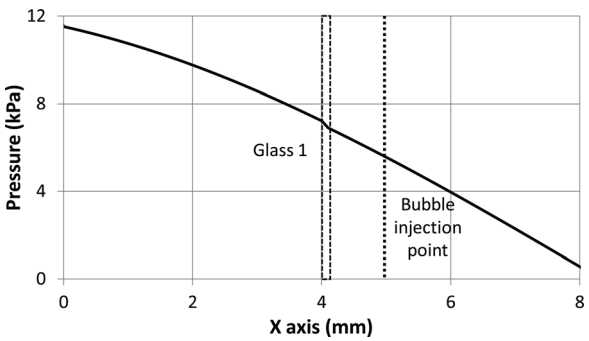

FIG. 4. A simulated pressure distribution in the water layer with glass 1 at 46.8 kHz for input amplitude of 4 V. The position of glass 1 is indicated by the dashed square and the bubble injection point is shown by the dotted line.

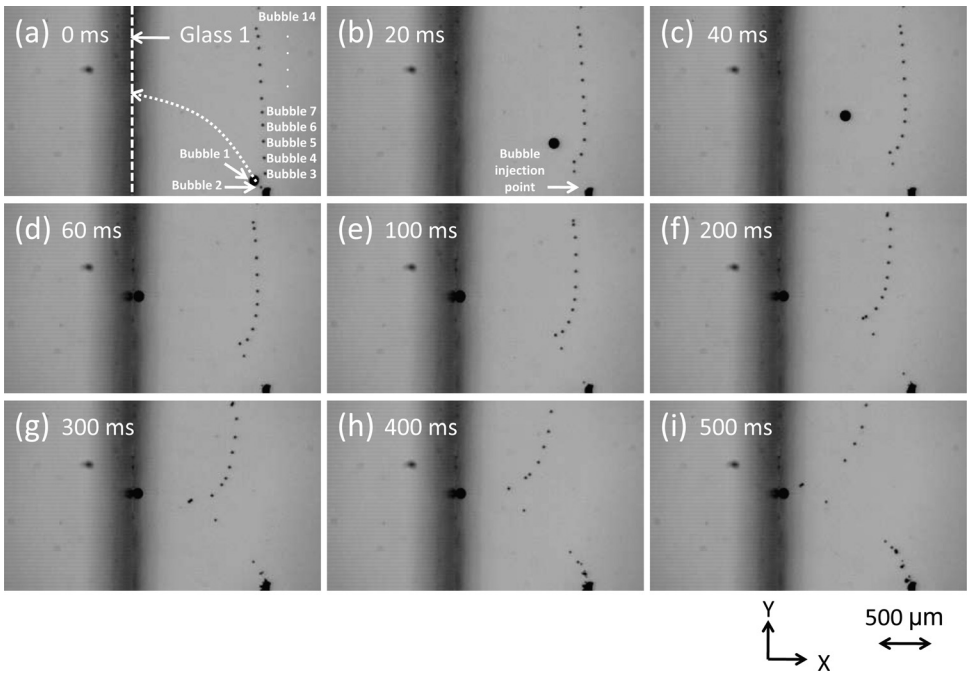

FIG. 5. Selected frames from a video showing the translations of several bubbles from the injection point to glass 1 at (a) 0 ms, (b) 20 ms, (c) 40 ms, (d) 60 ms, (e) 100 ms, (f) 200 ms, (g) 300 ms, (h) 400 ms, and (i) 500 ms. The pressure amplitude was 11.5 kPa.

Also, the presence of glass 1 creates a pressure drop between its two sides (from 7.3 kPa at $x = 4$ to 6.9 kPa at $x = 4.1$ mm).

It needs to be noted here that the resonance frequency of a bubble attached to a wall is different from that in a free space as presented by Eq. (13). The influence of a wall on the bubble resonance frequency, however, is directly related to the separation distance between the bubble and the wall. For a bubble oscillating near a surface, its angular resonance

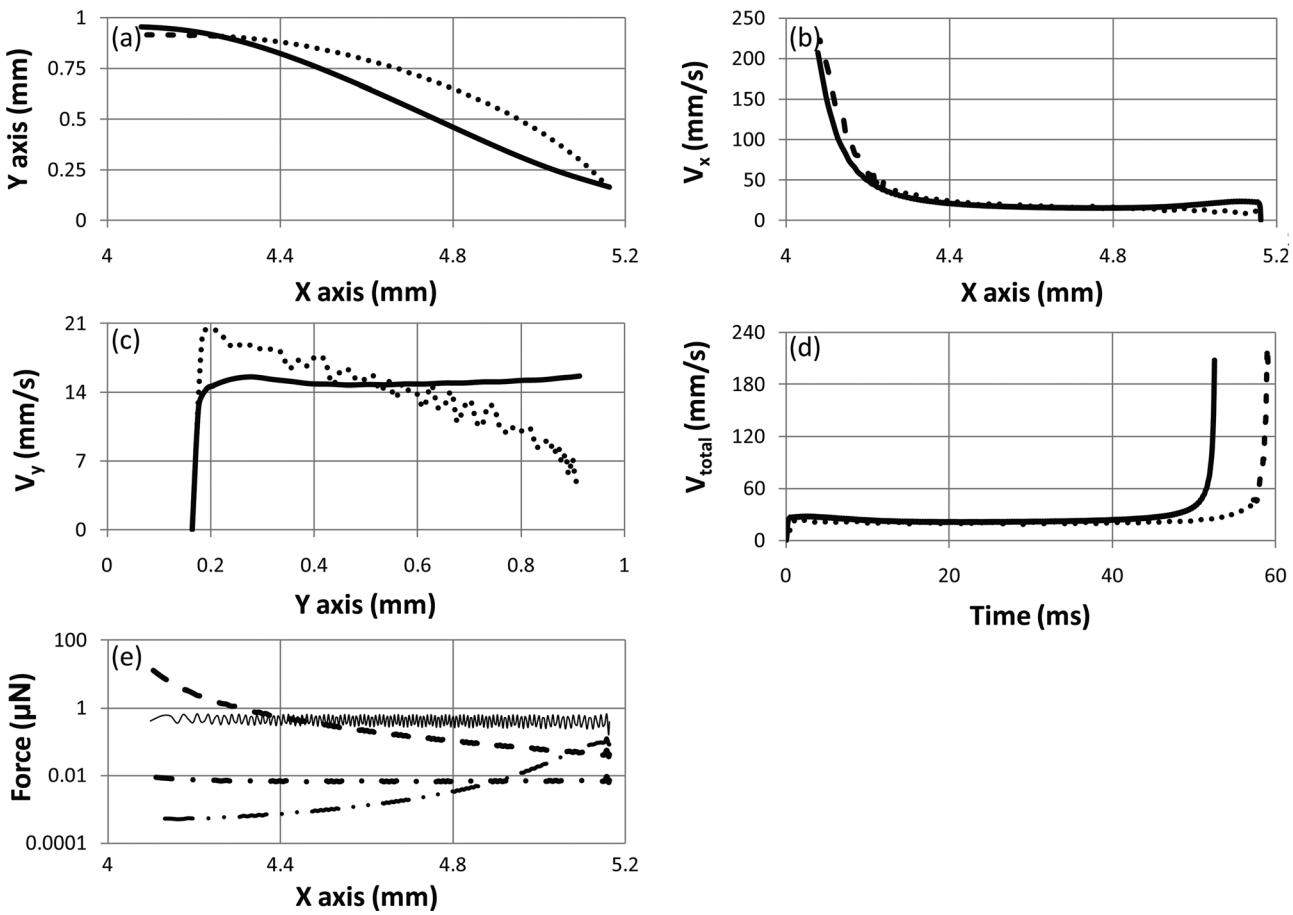

FIG. 6. The translation of bubble 1 at 46.8 kHz (a) bubble trajectory: …, experimental result; –, theoretical prediction; (b) velocity in the x axis: …, experimental result; –, theoretical prediction; (c) velocity in the y axis: …, experimental result; –, theoretical prediction; (d) total velocity: …, experimental result; –, theoretical prediction; (e) relationship between different forces: –, primary Bjerknes force; -|-, secondary Bjerknes force from glass 1, –··–, secondary Bjerknes force from glass 2; –·–, secondary Bjerknes force from bubble 2. The pressure amplitude was 11.5 kPa.

frequency (ω_{wall}) is related to the free resonance frequency (ω_0) by $\omega_{wall} \sim \omega_0/\sqrt{1+2R_0/d_w}$, where d_w is the separation distance from the wall.[43,44] The initial separation distances as shown in the present study were at least 10 times larger than the bubble diameter; this means the ω_{wall} would be approximately equal to its free space resonance. Moreover, the bubbles were driven well below their resonance frequencies, and their sizes were considered to be relatively small. Thus the bubbles were anticipated to translate toward the glass 1 from the bubble injection point at $x = 5$ mm.

B. Bubble translation in the acoustic standing wave field

The translations of several bubbles moving from the bubble injection point toward glass 1 (Fig. 1) are displayed in Fig. 5 at a pressure amplitude of 11.5 kPa. The radius of bubble 1 in Fig. 5 is 42 μm, and the radii of the other bubbles are around 13 μm.

Initially, bubble 1 moves toward glass 1 at a faster speed than bubbles 2–14. After 60 ms, bubble 1 first arrives on glass 1, while the bubbles 2–14 are moving on trajectories toward glass 1 and are starting to form an arrow shape in the liquid medium. Bubbles 3 and 4 are the first two to merge with bubble 1 at 400 ms followed by bubbles 5, 2, 6, and 7 sequentially.

V. DISCUSSION

The translation of a bubble in a liquid medium is the outcome of the competition of different external forces. The bubble motion is sensitive to the changes of surrounding environment such as the presence of neighboring bubbles and boundary surfaces. In this section, the translations of bubbles are investigated by analyzing the relationship between acoustic and hydrodynamic forces exerted on the bubbles. All the bubble translations shown in Fig. 5 were studied, and bubbles 1, 3, 5, and 7 are chosen here to illustrate the force relationship. The influence of bubble size and pressure amplitude on the bubble translation is also explored.

A. The translation of bubble 1

Recalling the force analysis in Sec. III, the translation of bubble 1 can be examined in the x and y axes, respectively, and the relationship of several main external forces in the x axis is shown in Fig. 6(e).

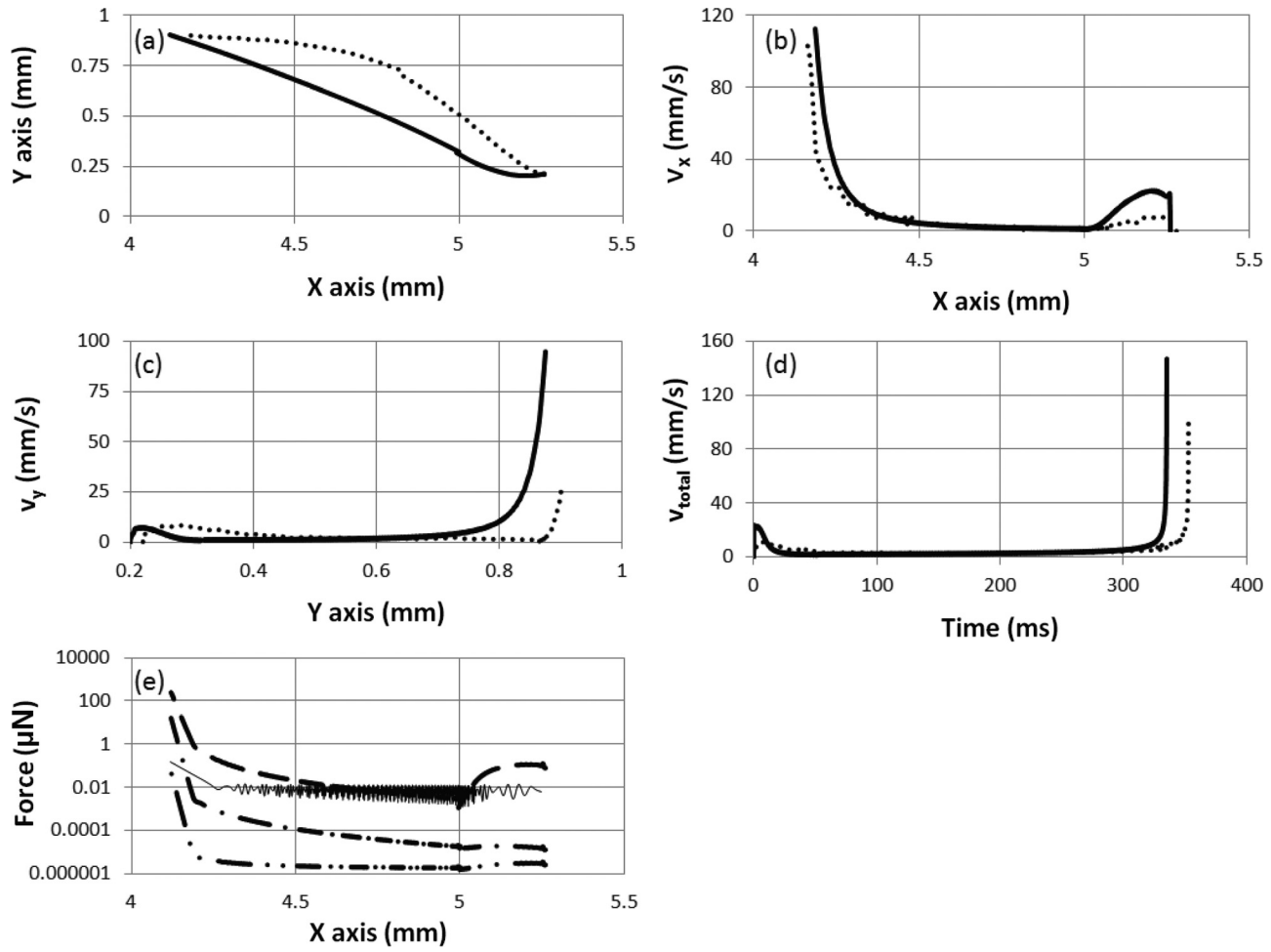

FIG. 7. The translation of bubble 3 at 46.8 kHz (a) bubble trajectory: …, experimental result; –, theoretical prediction; (b) velocity in the x axis: …, experimental result; –, theoretical prediction; (c) velocity in the y axis: …, experimental result; –, theoretical prediction; (d) total velocity: …, experimental result; –, theoretical prediction; (e) relationship between different forces: –, primary Bjerknes force; -|-, secondary Bjerknes force from glass 1; –··–, secondary Bjerknes force from glass 2; %, secondary Bjerknes force from bubble 2. The pressure amplitude was 11.5 kPa.

In the x axis, after the ultrasound is switched on, bubble 1 is mainly controlled by the primary Bjerknes force and starts to move in the direction toward glass 1 from the bubble injection point. It can be seen from Fig. 6(b) that the velocity of bubble 1 in the x axis suddenly rises from 0 to 16 mm/s at $x = 5.15$ mm and then maintains the speed until arriving at $x = 4.4$ mm. After that, the secondary Bjerknes force from glass 1 grows stronger and starts to outweigh the primary Bjerknes force. The secondary Bjerknes force from glass 2 and a nearby bubble 2 can be neglected at this stage. The velocity of bubble 1 surges up from 20 mm/s at $x = 4.4$ mm to 207 mm/s at $x = 4.07$ mm. Good agreement is found between the experiment and theoretical prediction of the bubble 1 x axis velocity.

In the y axis, it is anticipated that the buoyancy force is stronger than the drag force at the beginning, but later on a balance is reached between the two forces. From theory, bubble 1 is expected to move at a steady speed of 15 mm/s after taking off from the bubble injection point. However, in the experiment, the velocity of bubble 1 witnesses a rise from 0 mm/s at $y = 0.16$ mm to 20 mm/s at $y = 0.18$ mm followed by a gradual drop to 6 mm/s at $y = 0.89$ mm. From the point of view of force, it is possible that the primary Bjerknes force on bubble 1 is weaker than expected because the standing wave field has not been fully established at the moment when the sound field is switched on. In the later phase, especially when bubble 1 is moving close to glass 1, the full strength primary Bjerknes force and the attractive force from glass 1 greatly accelerate the bubble motion in the x axis; this in turn shortens the traveling distance in the y axis over the same period. The velocity in the y axis, therefore, is decreasing when bubble 1 is approaching glass 1. This effect can also be seen in the time lag of the traveling time between theory and experiment [Fig. 6(d)]. In the experiment, the time for bubble 1 to move from the bubble injection point to glass 1 is 60 ms, which is longer than the 52 ms from the theory due to the insufficient primary Bjerknes force experienced by bubble 1 at the beginning.

B. The translations of bubbles 3, 5, and 7

It can be seen from Fig. 5 that bubbles 2–14 move at a much slower speed than bubble 1, and their translations behave in a different manner. To explain such behavior, bubbles 3, 5, and 7 are chosen here as the example bubbles because they represent the typical translational behavior experienced by all other bubbles.

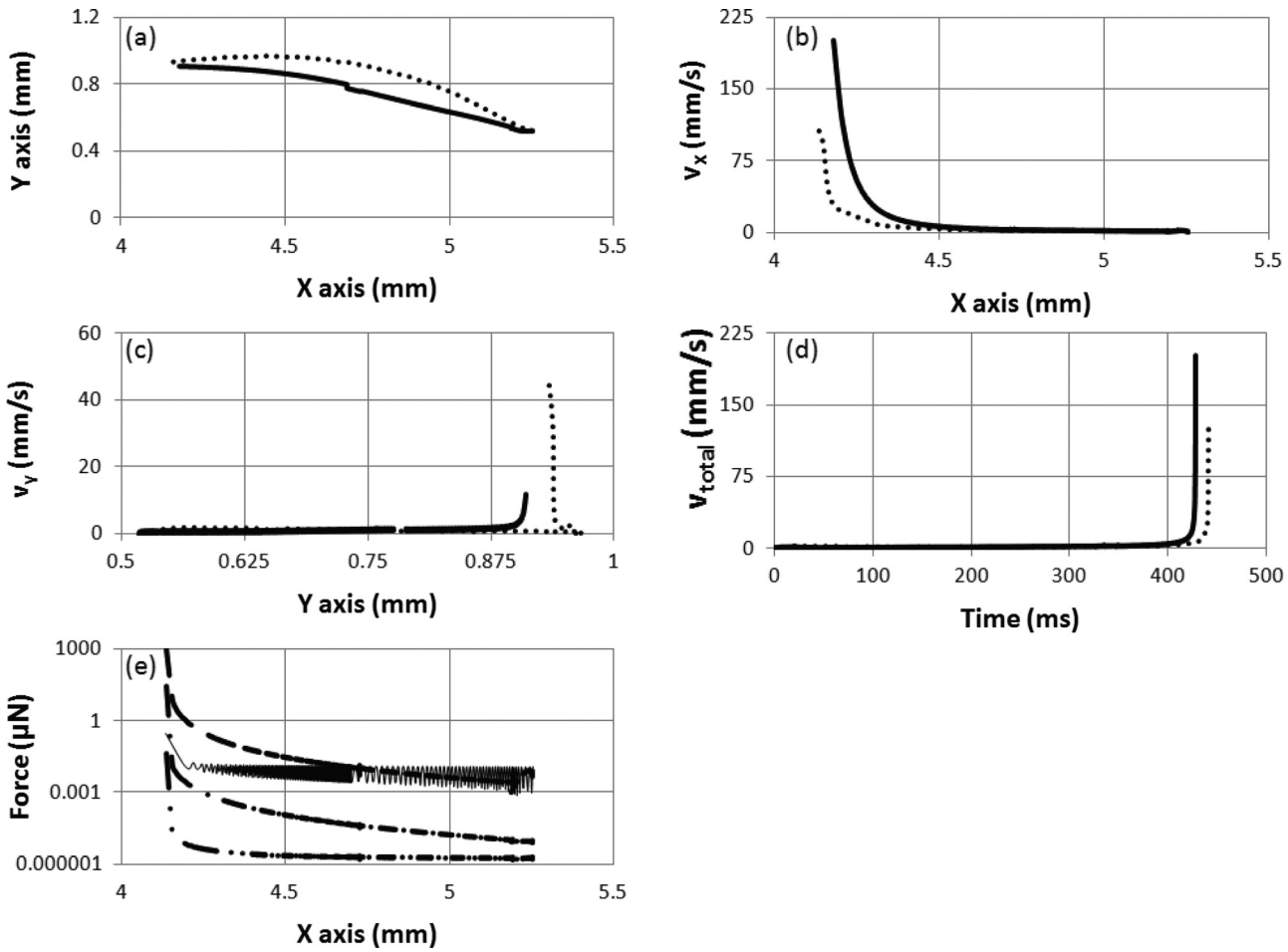

FIG. 8. The translation of bubble 5 at 46.8 kHz (a) bubble trajectory: …, experimental result; –, theoretical prediction; (b) velocity in the x axis: …, experimental result; –, theoretical prediction; (c) velocity in the y axis: …, experimental result; –, theoretical prediction; (d) total velocity: …, experimental result; –, theoretical prediction; (e) relationship between different forces: –, primary Bjerknes force; -|-, secondary Bjerknes force from glass 1; –··–, secondary Bjerknes force from glass 2; –··–, secondary Bjerknes force from bubble 2. The pressure amplitude was 11.5 kPa.

By decomposing the external forces into the x axis force and y axis force, one can study the bubble translation using the same procedure as for bubble 1. Initially, the motion of bubble 3 in the x axis, for example, is mainly controlled by the secondary Bjerknes force from bubble 1. When bubbles 1 and 3 are still close to each other, this secondary Bjerknes force is stronger than the primary Bjerknes force and results in a surge in velocity in the x axis [Fig. 7(b)]. As bubble 1 is moving at a faster speed toward glass 1, the distance between bubbles 3 and 1 grows to the extent that such bubble–bubble interaction is weaker than the primary Bjerknes force. The predicted velocity in the x axis, therefore, decreases from 20 mm/s at $x = 5.25$ mm to 4 mm/s at $x = 5$ mm, while in the experiment the change of velocity over the same period is smaller than the expectation but is still noticeable. From Fig. 7(a), it can be seen that the predicted trajectory of bubble 3 between $x = 5.25$ mm to $x = 5$ mm also deviates from the experimental result. As discussed in the bubble 1 case, at the beginning of the experiment, the standing wave field in the experiment is weaker than the theoretical prediction, which forces bubble 1 to move away from the anticipated trajectory. The trajectory of bubble 3 is consequently changed because the secondary Bjerknes force between bubble 1 and 3 dominates the translation of bubble 3 over that period. However, the shape of the velocity profile between $x = 5.25$ mm and $x = 5$ mm in the experiment is still consistent with that of the theory.

After the arrival of bubble 1 on to glass 1, the primary Bjerknes force and the secondary Bjerknes force from bubble 1 become the major factors that control the translation of bubble 3. The velocity of bubble 3 in the x axis between $x = 5$ mm and $x = 4.5$ mm is around 3 mm/s. When the distance between bubble 3 and bubble 1 decreases, the secondary Bjerknes force from bubble 1 is again dominating the motion of bubble 3 in the x axis. Moreover, within the near field of bubble 1, the secondary Bjerknes force from glass 1 becomes stronger than the primary Bjerknes force and contributes to the boost of velocity along with the interaction force between bubbles 1 and 3. The velocity of bubble 3 jumps from 3 mm/s at $x = 4.5$ mm/s to 90 mm/s at $x = 4.18$ mm, which is close to the predicted 112 mm/s.

In the y axis, initially, bubble 3 is lifted by the attractive force from bubble 1 and the buoyancy force. As bubble 1 is moving away at a faster speed, the bubble 1 and 3 interaction diminishes as a function of time, and the bubble 3 y axis velocity remains at 3 mm/s between $y = 0.17$ mm and $y = 0.7$ mm in Fig. 7(c). After that, the attractive force from

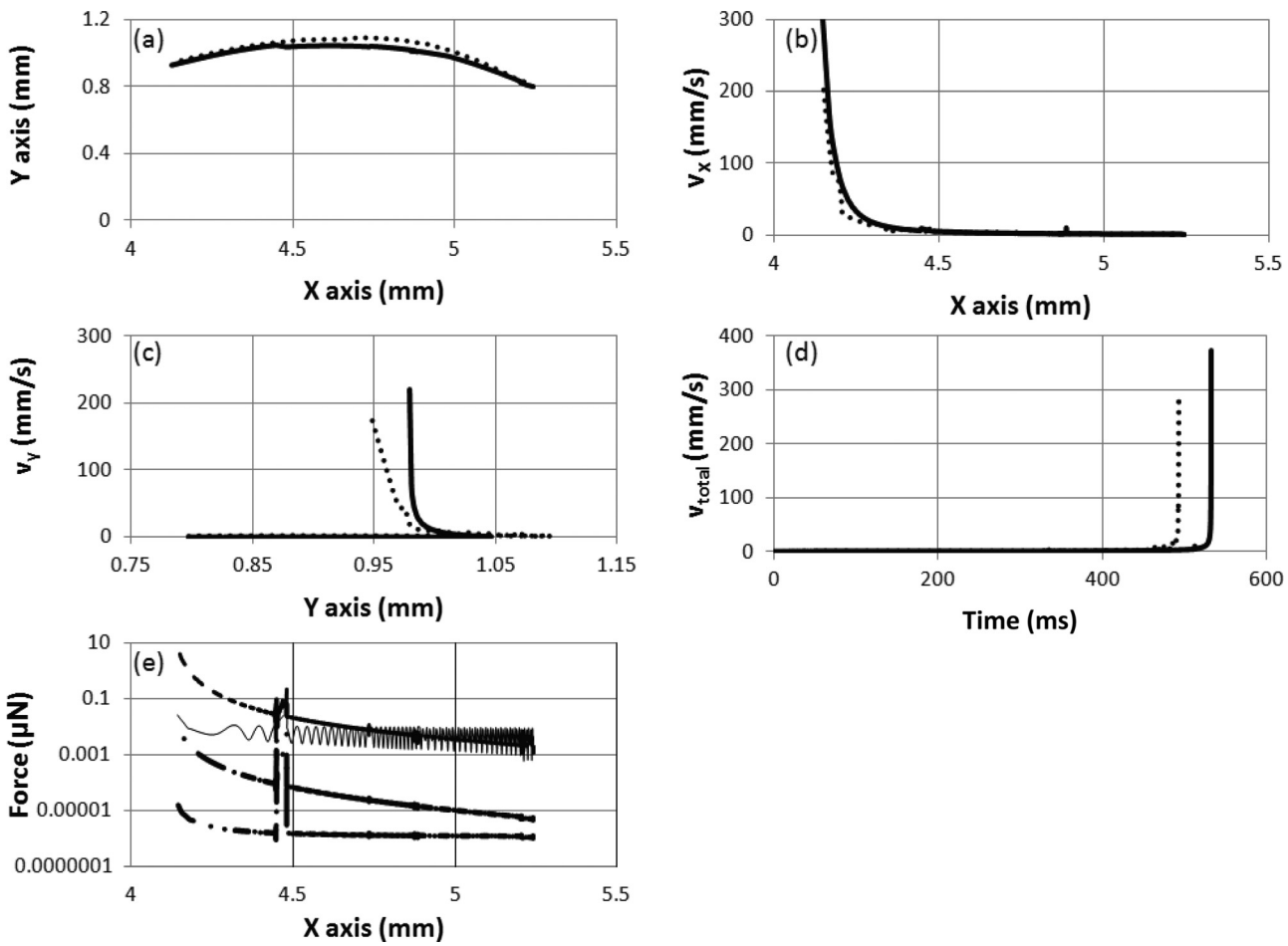

FIG. 9. The translation of bubble 7 at 46.8 kHz (a) bubble trajectory: …, experimental result; –, theoretical prediction; (b) velocity in the x axis: …, experimental result; –, theoretical prediction; (c) velocity in the y axis: …, experimental result; –, theoretical prediction; (d) total velocity: …, experimental result; –, theoretical prediction; (e) relationship between different forces: –, primary Bjerknes force; -|-, secondary Bjerknes force from glass 1; –··–, secondary Bjerknes force from glass 2; –··–, secondary Bjerknes force from bubble 2. The pressure amplitude was 11.5 kPa.

bubble 1 significantly accelerates the velocity when bubble 3 approaches bubble 1. A 94 mm/s velocity is seen in the theoretical prediction at $y = 0.88$ mm, which is higher than the 27 mm/s one observed in the experiment. Because bubble 3 moves on a trajectory that is not perfectly matching the theoretical prediction, the consequent bubble translation, especially at the moment when bubbles 1 and 3 are close enough, could be different from what is expected from theory. Therefore, the y axis velocity in the experiment is different from that of the simulation. The predicted overall traveling time for bubble 3 to move from the bubble injection point to glass 1 is in quantitative agreement with the experimental result as shown in Fig. 7(d).

A similar analysis was also applied to bubbles 5 and 7 in Figs. 8 and 9, respectively. A surge of x axis velocity due to the increase of secondary Bjerknes force from the surface is seen for both bubbles in Figs. 8(b) and 9(b). The observed maximum x axis velocity of bubbles 5 and 7 are 109 and 214 mm/s, which are lower than the anticipated 200 and 300 mm/s from the model. Ideally, the detection of velocity change, especially at the moment when the bubble is approaching the boundary, requires a high frame rate. However, the limited frame rate used in the experiment was unable to provide the small time interval to construct the accurate velocity information at the final moment when the bubble contacting the surface and therefore results in a lower than expected x axis velocity in Figs. 8(b) and 9(b).

It needs to be pointed out here that the influence from bubble 1 on the nearby bubbles decreases with an increase of distance between the bubbles. For the bubbles in the far field of bubble 1, a weaker attractive force generated from bubble 1 was anticipated. It can be seen from Fig. 9 that because bubble 7 moves at a slow speed, the standing wave field has sufficient time to be established in the x axis. The predicted translation of bubble 7, therefore, is in good agreement with the experimental result. On the other hand, there is a discrepancy of bubble trajectory between the experiment and the prediction for bubble 5 in Fig. 8(a) that is the consequence of the deviation between the observed and calculated trajectory of bubble 1 shown in Fig. 6(a).

C. Parametric study

To transport a large amount of bubbles of given size to an appointed position on a surface, one needs to optimize the

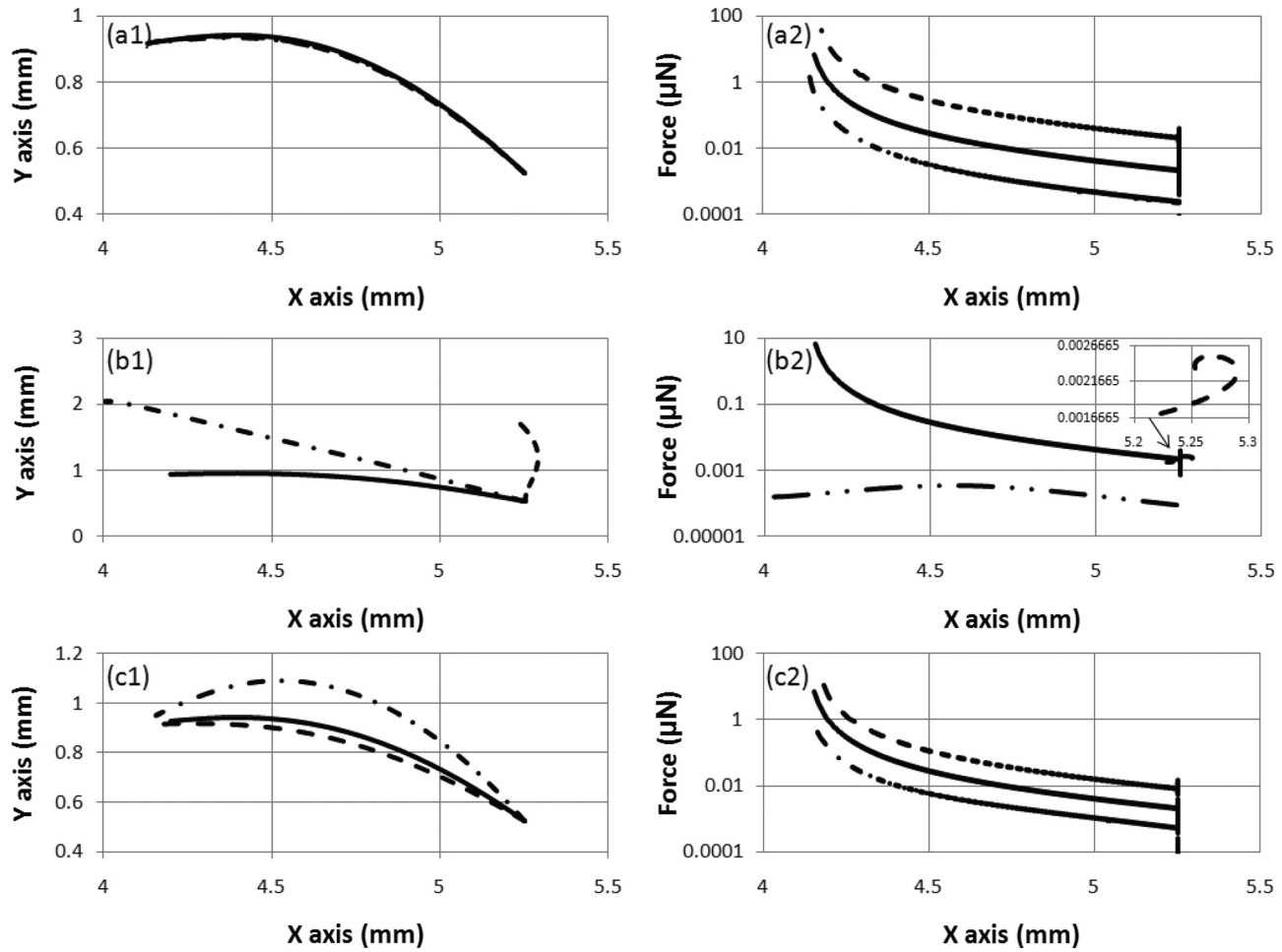

FIG. 10. A parametric study of the bubble translation under different conditions. The calculated forces are represented by their absolute values. (a1) at 11.5 kPa, the radii of bubble 2 are 6.5 μm (–·–), 13 μm (-), and 26 μm (– –); (a2) at 11.5 kPa, the secondary Bjerknes force on bubble 2 with radii of 6.5 μm (–·–), 13 μm (-), and 26 μm (– –); (b1) at 11.5 kPa, the radii of bubble 1 are 25 μm (–·–), 50 μm (–), and 100 μm (– –); (b2) at 11.5 kPa, the secondary Bjerknes force on bubble 2 with bubble 1 of radii of 25 μm (–·–), 50 μm (–), and 100 μm (– –). The secondary force between the 100 μm bubble 1 and 13 μm bubble 2 is shown in the inset; (c1) for a pair of bubbles of radii of 50 μm and 13 μm, the pressure amplitude is 5.25 kPa (–·–), 11.5 kPa (—), and 23 kPa (– –); (c2) the secondary Bjerknes force between the bubbles at 5.22 kPa (–·–), 11.5 kPa (–), and 23 kPa (– –).

external forces exerted on the bubbles, such as primary and secondary Bjerknes forces. In Sec. III, it is seen that the Bjerknes forces are directly related to the bubble size and external pressure amplitude. In this section, the influence of different bubble sizes and pressure amplitudes on the bubble translation is discussed.

The translation of the 13 μm bubbles are sensitive to the changes of acoustic and hydrodynamic forces. Let us assume a bubble 1 of radius of 42 μm is fixed on glass 1 at $x = 4$ mm, $y = 0.9$ mm, and another bubble 2 can move freely in the water layer. The driving frequency is kept at 46.8 kHz. The calculated forces in Figs. 10(a2), 10(b2) and 10(c2) are represented by their absolute values.

First, three radii of bubble 2, 6.5, 13, and 26 μm, are used in Figs. 10(a1) and 10(a2) at 11.5 kPa. Figure 10(a1) shows that changing the radius of bubble 2 can hardly alter its trajectory. The secondary Bjerknes force between bubbles 1 and 2 is proportional to their sizes and therefore an increase of the size of bubble 2 results in an increase of secondary Bjerknes force as well; this in turn accelerates the velocity of bubble 2. The traveling time of bubble 2 was found from our calculations to be shortened from 2500 ms for the 6.5 μm bubble to 100 ms for the 26 μm one.

Second, the radius of bubble 2 is assumed to be 13 μm, and the radius of bubble 1 is varying from 25 to 100 μm. The pressure amplitude is 11.5 kPa. A striking difference of bubble 2 trajectory is noticed in Fig. 10(b1). Bubble 2 experiences much less secondary Bjerknes force from the 25 μm bubble 1 than from the 100 μm one. The 100 μm bubble exerts a repulsive instead of attractive force on bubble 2. It is well known that the secondary Bjerknes force between two bubbles can shift from an attractive force when the bubbles are oscillating in phase to a repulsive force when their oscillations are out of phase.[28,39] Based on Eq. (13), at 46.8 kHz, the 100 μm bubble is driven above its resonance frequency, while bubble 2 is smaller than the resonance size. Therefore, the secondary Bjerknes force between these two bubbles shifts from an attractive one to a repulsive one in the 100 μm (bubble 1) case.

Third, the radii of bubbles 1 and 2 are kept as 42 and 13 μm, respectively. The pressure amplitude is increased from 5.25 to 23 kPa [Figs. 10(c1) and 10(c2)]. At a lower pressure amplitude, bubble 2 experiences a smaller secondary Bjerknes force from bubble 1, which only starts to divert the trajectory of bubble 2 within the near field [Fig. 10(c1)]. At a higher pressure amplitude, the bubble 2 migrates directly toward bubble 1 at a faster speed due to the increase of interaction between the bubbles [Fig. 10(c2)].

VI. CONCLUSION

The collective bubble dynamics near a surface in a weak acoustic standing wave field is shown. The bubble translation in a multi-bubble environment was achieved by using a multi-layered resonator that created an uniform one-dimensional acoustic standing wave field in a water layer. The bubble motion was modeled by a pair of modified Keller–Miksis equation and bubble translation equation. The influence of several acoustic and hydrodynamic forces on the bubble translation was investigated. It was found that the bubble translation near a surface in a multi-bubble environment was mainly controlled by the primary Bjerknes force imposed by the acoustic field, secondary Bjerknes forces introduced by a surface and neighboring bubbles, and buoyancy force from the surrounding liquid. The primary Bjerknes force dominated the bubble translation when the bubble was far away from the surface and was outweighed by the secondary Bjerknes force from the boundary when the bubble was approaching the surface. Moreover, a strong secondary Bjerknes force generated by a neighboring bubble was noticed in the experiment. The bubble–bubble interaction forced nearby bubbles to move on trajectories toward the target bubble instead of the positions that they would have moved to in the absence of the target bubble. It was also seen from a parametric study that increasing the pressure amplitude can enhance the interaction between two bubbles and force bubbles to move at a faster speed. The secondary Bjerknes force between two bubbles can shift from an attractive one when two bubbles oscillate in phase to a repulsive one when their oscillations are out of phase. All of these effects can be decided quantitatively with the presented theory.

ACKNOWLEDGMENTS

X.X. and F.C. would like to acknowledge financial support from Lam Research AG (SEZ-Strasse 1, 9050 Villach, Austria). R.M gratefully acknowledges financial support by the Austrian Federal Ministry of Economy, Family, and Youth and the Austrian National Foundation for Research, Technology and Development.

[1] A. Vogel, W. Lauterborn, and R. Timm, "Optical and acoustic investigations of the dynamics of laser-produced cavitation bubbles near a solid boundary," J. Fluid Mech. **206**, 299–338 (1989).
[2] J. Blake and D. Gibson, "Cavitation bubbles near boundaries," Annu. Rev. Fluid Mech. **19**, 99–123 (1987).
[3] O. Lindau and W. Lauterborn, "Cinematographic observation of the collapse and rebound of a laser-produced cavitation bubble near a wall," J. Fluid Mech. **479**, 327–348 (2003).
[4] P. Prentice, A. Cuschieri, K. Dholakia, M. Prausnitz, and P. Campbell, "Membrane disruption by optically controlled microbubble cavitation," Nat. Phys **1**, 107–110 (2005).
[5] A. Philipp, M. Delius, C. Scheffczyk, A. Vogel, and W. Lauterborn, "Interaction of lithotripter-generated shock waves with air bubbles," J. Acoust. Soc. Am. **93**, 2496–2509 (1993).
[6] A. Philipp and W. Lauterborn, "Cavitation erosion by single laser-produced bubbles," J. Fluid Mech. **361**, 75–116 (1998).
[7] C. Ohl, M. Arora, R. Dijkink, V. Janve, and D. Lohse, "Surface cleaning from laser-induced cavitation bubbles," Appl. Phys. Lett. **89**, 074102 (2006).
[8] W. Kim, T. Kim, J. Choi, and H. Kim, "Mechanism of particle removal by megasonic waves," Appl. Phys. Lett. **94**, 081908 (2009).
[9] W. Song, M. Hong, B. Lukyanchuk, and T. Chong, "Laser-induced cavitation bubbles for cleaning of solid surfaces," J. Appl. Phys. **95**, 2952–2956 (2004).
[10] M. Plesset and R. Chapman, "Collapse of an initially spherical vapour cavity in the neighbourhood of a solid boundary," J. Fluid Mech. **47**, 283–290 (1971).
[11] K. Sato, Y. Tomita, and A. Shima, "Numerical analysis of a gas bubble near a rigid boundary in an oscillatory pressure field," J. Acoust. Soc. Am. **95**, 2416–2424 (1994).
[12] J. Blake, G. Keen, R. Tong, and M. Wilson, "Acoustic cavitation: The fluid dynamics of non-spherical bubbles," Philos.Trans. R. Soc. London, Ser. A **357**, 251–267 (1999).

[13]W. Lauterborn and T. Kurz, "Physics of bubble oscillations," Rep. Prog. Phys. **73**, 106501 (2010).
[14]X. Xi, F. Yang, D. Chen, Y. Luo, D. Zhang, N. Gu, and J. Wu, "A targeting drug-delivery model via interactions among cells and liposomes under ultrasonic excitation," Phys. Med. Biol. **53**, 3251–3265 (2008).
[15]P. Marmottant and S. Hilgenfeldt, "Controlled vesicle deformation and lysis by single oscillating bubbles," Nature **423**, 153–156 (2003).
[16]P. Marmottant, S. van der Meer, M. Emmer, M. Versluis, N. de Jong, S. Hilgenfeldt, and D. Lohse, "A model for large amplitude oscillations of coated bubbles accounting for buckling and rupture," J. Acoust. Soc. Am. **118**, 3499–3505 (2005).
[17]P. Marmottant, M. Versluis, N. de Jong, S. Hilgenfeldt, and D. Lohse, "High-speed imaging of an ultrasound-driven bubble in contact with a wall: 'Narcissus' effect and resolved acoustic streaming," Exp. Fluids **41**, 147–153 (2006).
[18]V. Garbin, D. Cojoc, E. Ferrari, E. Di Fabrizio, M. Overvelde, S. van Der Meer, N. de Jong, D. Lohse, and M. Versluis, "Changes in microbubble dynamics near a boundary revealed by combined optical micromanipulation and high-speed imaging," Appl. Phys. Lett. **90**, 114103 (2007).
[19]H. Vos, B. Dollet, J. Bosch, M. Versluis, and N. de Jong, "Nonspherical vibrations of microbubbles in contact with a wall-a pilot study at low mechanical index," Ultrasound Med. Biol. **34**, 685–688 (2008).
[20]H. Vos, B. Dollet, M. Versluis, and N. de Jong, "Nonspherical shape oscillations of coated microbubbles in contact with a wall," Ultrasound Med. Biol. **37**, 935–948 (2011).
[21]A. Doinikov, J. Haac, and P. Dayton, "Modeling of nonlinear viscous stress in encapsulating shells of lipid-coated contrast agent microbubbles," Ultrasonics **49**, 269–275 (2009).
[22]A. Doinikov and A. Bouakaz, "Theoretical investigation of shear stress generated by a contrast microbubble on the cell membrane as a mechanism for sonoporation," J. Acoust. Soc. Am. **128**, 11–19 (2010).
[23]A. Doinikov and A. Bouakaz, "Acoustic microstreaming around a gas bubble," J. Acoust. Soc. Am. **127**, 703–709 (2010).
[24]L. King, "On the acoustic radiation pressure on spheres," Philos. Trans. R. Soc. London, Ser. A **147**, 212–240 (1934).
[25]A. Eller, "Force on a bubble in a standing acoustic wave," J. Acoust. Soc. Am. **43**, 170–171 (1968).
[26]L. Crum, "Bjerknes forces on bubbles in a stationary sound field," J. Acoust. Soc. Am. **57**, 1363–1370 (1975).
[27]J. Rensen, D. Bosman, J. Magnaudet, C. Ohl, A. Prosperetti, R. Togel, M. Versluis, and D. Lohse, "Spiraling bubbles: How acoustic and hydrodynamic forces compete," Phys. Rev. Lett. **86**, 4819–4822 (2001).
[28]I. Akhatov, R. Mettin, C. Ohl, U. Parlitz, and W. Lauterborn, "Bjerknes force threshold for stable single bubble sonoluminescence," Phys. Rev. E **55**, 3747–3750 (1997).
[29]P. Koch, T. Kurz, U. Parlitz, and W. Lauterborn, "Bubble dynamics in a standing sound field: The bubble habitat," J. Acoust. Soc. Am. **130**, 3370–3378 (2011).
[30]T. Barbat, N. Ashgriz, and C. Liu, "Dynamics of two interacting bubbles in an acoustic field," J. Fluid Mech. **389**, 137–168 (1999).
[31]A. Doinikov and S. Zavtrak, "On the mutual interaction of two gas bubbles in a sound field," Phys. Fluids **7**, 1923–1930 (1995).
[32]R. Mettin, I. Akhatov, U. Parlitz, C. Ohl, and W. Lauterborn, "Bjerknes forces between small cavitation bubbles in a strong acoustic field," Phys. Rev. E **56**, 2924–2931 (1997).
[33]R. Mettin, S. Luther, C. Ohl, and W. Lauterborn, "Acoustic cavitation structures and simulations by a particle model," Ultrason. Sonochem. **6**, 25–30 (1999).
[34]U. Parlitz, R. Mettin, S. Luther, I. Akhatov, M. Voss, and W. Lauterborn, "Spatio-temporal dynamics of acoustic cavitation bubble clouds," Philos. Trans. R. Soc. London, Ser. A **357**, 313–334 (1999).
[35]A. Doinikov, "Mathematical model for collective bubble dynamics in strong ultrasound fields," J. Acoust. Soc. Am. **116**, 821–827 (2004).
[36]X. Xi, F. Cegla, M. Lowe, A. Thiemann, T. Nowak, R. Mettin, F. Holsteyns, and A. Lippert, "Study on the bubble transport mechanism in an acoustic standing wave field," Ultrasonics **51**, 1014–1025 (2011).
[37]P. Wilcox, R. Monkhouse, P. Cawley, M. Lowe, and B. Auld, "Development of a computer model for an ultrasonic polymer film transducer system," NDT&E.INT **31**, 51–64 (1998).
[38]M. Hill, Y. Shen, and J. Hawkes, "Modelling of layered resonators for ultrasonic separation," Ultrasonics **40**, 385–392 (2002).
[39]T. Leighton, *The Acoustic Bubble* (Academic Press, London, 1997), Chap. 3, pp. 181–183.
[40]B. Krasovitski and E. Kimmel, "Gas bubble pulsation in a semiconfined space subjected to ultrasound," J. Acoust. Soc. Am. **109**, 891–898 (2001).
[41]A. Doinikov, "Translational motion of a spherical bubble in an acoustic standing wave of high intensity," Phys. Fluids **14**, 1420–1425 (2002).
[42]J. Keller and M. Miksis, "Bubble oscillations of large amplitude," J. Acoust. Soc. Am. **68**, 628–633 (1980).
[43]M. Strasberg, "The pulsation frequency of nonspherical gas bubbles in liquids," J. Acoust. Soc. Am. **25**, 536–537 (1953).
[44]E. Payne, S. Illesinghe, A. Ooi, and R. Manasseh, "Symmetric mode resonance of bubbles attached to a rigid boundary," J. Acoust. Soc. Am. **118**, 2841–2849 (2005).